Hindawi Publishing Corporation
International Journal of Photoenergy
Volume 2014, Article ID 394146, 7 pages
http://dx.doi.org/10.1155/2014/394146

Research Article

Surfactant-Free Synthesis of Single Crystalline SnS_2 and Effect of Surface Atomic Structure on the Photocatalytic Property

Mengyi Li,[1] Enzuo Liu,[1,2] Huilin Hu,[1] Shuxin Ouyang,[1,2] Hua Xu,[1,2] and Defa Wang[1,2]

[1] *TU-NIMS Joint Research Center and Tianjin Key Laboratory of Composite and Functional Materials, School of Materials Science and Engineering, Tianjin University, 92 Weijin Road, Nankai District, Tianjin 300072, China*
[2] *Collaborative Innovation Center of Chemical Science and Engineering, 92 Weijin Road, Nankai District, Tianjin 300072, China*

Correspondence should be addressed to Defa Wang; defawang@tju.edu.cn

Received 14 July 2014; Accepted 8 September 2014; Published 1 December 2014

Academic Editor: Wenjun Luo

Sheetlike tin disulfide (SnS_2) single crystal exposed with well-defined {001} facets and flowerlike SnS_2 mainly exposed with {010} facets were prepared through a surfactant-free solvothermal process. Photocatalytic degradation of methyl orange (MO) under visible light irradiation indicated that the sheetlike SnS_2 showed a much higher activity than flowerlike SnS_2. Theoretical and experimental results revealed that the band structure derived from the surface atomic structure played a more important role than the surface energy in the photocatalytic property. The present work has provided a deep insight into the important role of the surface energy and band structure, both of which are derived from the surface atomic structure, in the photocatalytic activity.

1. Introduction

As an ideal green chemistry technology, semiconductor photocatalysis has been attracting extensive attention owing to its potential application in environment purification. The photocatalytic activity of a semiconductor is influenced by many factors, among which the surface atomic structure plays an important role. Generally speaking, the high energy facets that contain abundant unsaturated coordination atoms exhibit high reactivity [1–5]. For example, Yang et al. have found that the high energy {001} facets of anatase TiO_2 are much more reactive than the thermodynamically more stable low energy {010} facets [6]. Xi and Ye demonstrated that the well-defined $BiVO_4$ nanoplates with exposed {001} facets exhibited greatly enhanced activity for photocatalytic degradation of organic contaminants and for photocatalytic O_2 generation [7]. On the other hand, Pan et al. demonstrated that TiO_2 single crystal exposed with more {010} facets exhibited superior electronic band structure over that of TiO_2 exposed with more {001} facets, resulting in a higher photocatalytic activity [8]. Apparently, both the surface atomic geometry (atomic arrangement and coordination) and surface electronic structure play the crucial role in the photocatalytic activity of a semiconductor material.

Semiconducting metal sulfides are of an important kind of photocatalytic and photovoltaic materials. Among them, tin disulfide (SnS_2) has attracted considerable attention for applications in a variety of fields such as gas sensing [9], anode materials [10], and solar cell [11]. In addition to its low price, nontoxicity, and chemical stability in acidic or neutral solutions, hexagonal SnS_2 possesses a narrow band gap of 2.2–2.5 eV and has the potential to be a good visible-light photocatalyst [12–14]. Featured as a hexagonal CdI_2-type crystal structure consisting of S–Sn–S triple layer, in which the atomic layers are held together by weak van der Waals interactions, SnS_2 can be easily cleaved, allowing the formation of different morphologies [15]. To date, various SnS_2 morphologies, such as graphene-like [13], sphere-like [16], flower-like [17], nanotubes [18], nanoplates [19], nanobelts [20], and nanowires [21] structures, have been successfully fabricated by chemical bath, template methods, thermal decomposition, or hydrothermal methods and so on.

Herein we report for the first time a simple surfactant-free method for the preparation of sheetlike SnS_2 with exposed {001} facets and flowerlike SnS_2 with exposed {010} facets. Photocatalytic degradation of methyl orange (MO) under visible light irradiation indicated that the sheetlike SnS_2 showed a much higher activity than flowerlike SnS_2. Theoretical and

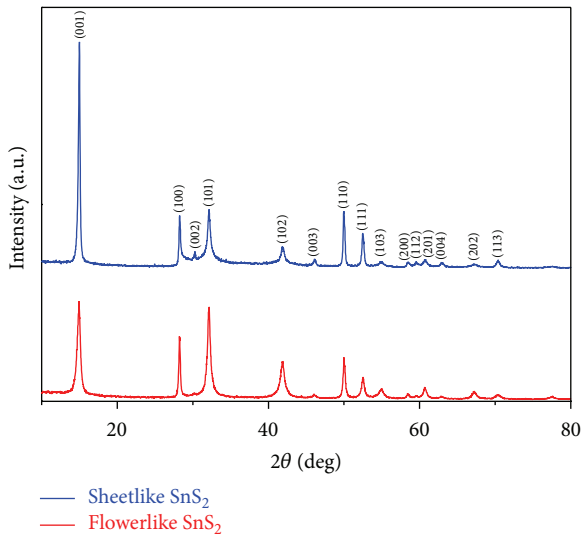

FIGURE 1: XRD patterns of the SnS_2 samples.

experimental results revealed that the band structure derived from the surface atomic structure played a more important role than the surface energy in the photocatalytic property.

2. Experimental

2.1. Photocatalyst Preparation. All reagents including tin chloride pentahydrate ($SnCl_4{\cdot}5H_2O$), concentrated hydrochloric acid, absolute alcohol, acetic acid, and thioacetamide (TAA) were analytical grade and used directly as received without further purification.

SnS_2 was prepared from $SnCl_4{\cdot}5H_2O$ (J&K) and TAA (J&K) via a solvothermal route. In a typical preparation, 5.0 mmol of $SnCl_4{\cdot}5H_2O$ was dissolved in 3 mL of concentrated hydrochloric acid (38%, w/w) in a 100 mL beaker. Then, 70 mL of deionized water and 12.5 mmol of TAA were added in sequence. After stirring, the reactants were transferred into a Teflon-line stainless steel autoclave of 100 mL capacity. The autoclave was sealed and heated at 180°C for 12 h and then cooled down to room temperature naturally. A yellow precipitate was collected and washed with deionized water and absolute ethanol for several times to remove the impurities. Finally, the sample was dried in vacuum at 60°C for 12 h to get the sheetlike SnS_2. To synthesize the flowerlike SnS_2, 5.0 mmol of $SnCl_4{\cdot}5H_2O$ was dissolved in 3 mL of acetic acid in a 100 mL beaker, and 70 mL of ethanol and 12.5 mmol of TAA were added in sequence. The following process was the same as that for sheetlike SnS_2 fabrication.

2.2. Characterization. Crystal structures of the as-prepared samples were determined by an X-ray diffractometer (XRD: D8 Advanced, Bruker, Germany) using Cu-Kα radiation (λ = 1.54178 Å) at a scanning rate of $0.02^\circ s^{-1}$. X-ray photoelectron spectroscopy (XPS) was performed on ThermoESCALAB250 using monochromatized Al Kα radiation as the exciting source, where the binding energies were calibrated by referencing the C 1s peak (284.6 eV). UV-vis diffuse reflectance spectra were measured at room temperature in the range of 220–800 nm on a UV-vis spectrophotometer (UV-vis DRS UV-2700, Shimadzu, Japan) by using $BaSO_4$ as reference and were converted to absorbance spectra by the Kubelka-Munk method. The Brunauer-Emmett-Teller (BET) surface areas were measured by a surface area analyzer (BET-BJH AsiQcovoo 2–4, Quantachrom, USA). Microstructures of the samples were observed on a scanning electron microscope (SEM S4800, Hitachi, Japan) and a transmission electron microscope (TEM Technai G2 F20, FEI, Netherlands).

2.3. Photocatalytic Activity Evaluation. Photocatalytic activity was evaluated by performing methyl orange (MO) degradation as follows: 40 mg of the catalyst was suspended in 100 mL of aqueous solution (10 mg/L) in a Pyrex reactor. Before irradiation, the suspension was stirred in the dark for about 2 h to ensure an adsorption-desorption equilibrium. Then the reaction was initiated by irradiating with a 300 W Xenon lamp located 15 cm away from the solution. A cutoff filter (L42, Hoya, Japan) was equipped to remove UV light. At a certain given time interval, 3 mL of reaction solution was sampled and separated by filter. The absorption spectrum of the filtrate was measured by UV-vis spectrophotometer.

2.4. Theoretical Calculations. Electronic structures and surface atomic structures of the two SnS_2 samples were investigated via the projector augmented wave (PAW) formalism of density functional theory as implemented in the Vienna Ab initio Simulation Package (VASP) [22]. The exchange-correlation function is approximated with the local density approximation (LDA). The energy cutoff for plane-wave expansion of the PAW's is 400 eV. As will be discussed below, {001} and {010} surfaces are modeled by periodically repeated slabs containing 6 and 7 SnS_2 layers, respectively, and separated by a vacuum region of more than 15 Å. The thickness of the slabs is determined when the energy of increased SnS_2 molecules with the thickness increasing approaches the energy of bulk SnS_2. We use a two-dimensional unit cell containing 1 and 4 SnS_2 per SnS_2 layer. The Brillouin zone is sampled using Monkhorst-Pack scheme [23] with 15 × 15 × 1 and 5 × 7 × 1 K-point grid for {001} and {010} surfaces, respectively. For geometry optimization, all the internal coordinates are relaxed until the Hellmann-Feynman forces are less than 0.01 eV/Å.

3. Results and Discussion

XRD patterns of the as-prepared SnS_2 samples are shown in Figure 1. We can see that all the peaks in the XRD patterns can be readily indexed to hexagonal SnS_2 with lattice constants a = 0.3648 nm and c = 0.5899 nm, which are in good agreement with the reported values (JCPDS file number 65-7657). No other impurity peaks were detected. Further analysis revealed that, for the sheetlike sample, the (001) diffraction peak showed the strongest intensity, indicating that the (001) orientation is predominant. For the flowerlike sample, the (001) diffraction peak remarkably decreased while the (101) peak relatively increased.

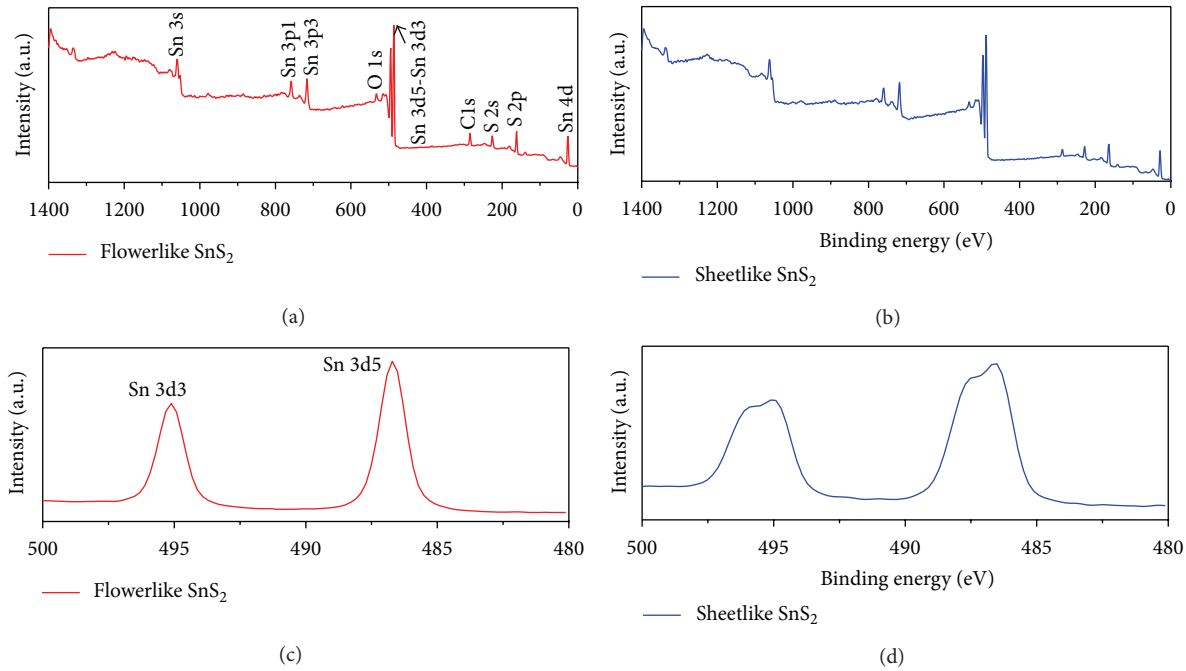

FIGURE 2: Wide range XPS survey profiles of the flowerlike SnS_2 (a) and sheetlike SnS_2 (b) and high-resolution spectra of Sn 3d in flowerlike SnS_2 (c) and sheetlike SnS_2 (d).

Meanwhile, the surface electronic states and the chemical composition of samples were detected by XPS. The survey spectra showed the presence of Sn, C, S, and O in both the sheetlike and flowerlike samples (see Figures 2(a) and 2(b)). The two strong peaks around 486.5 and 495 eV displayed in Figures 2(c) and 2(d) can be attributed to Sn $3d_{3/2}$ and $3d_{5/2}$, respectively, which are in good accordance with the characteristic peak of Sn(IV) [24]. No Sn^{2+} peak (binding energy at round 485.8 eV) was detected in the Sn 3d spectrum, indicating the formation of pure SnS_2.

The size and morphology of the obtained samples were observed by SEM, TEM, and HRTEM. Figure 3(a) presents a typical SEM image of the sheetlike SnS_2, which are 80–100 nm in width and 20–30 nm in thickness. TEM observation (Figure 3(b)) further confirmed the structural feature of the well-defined hexagonal plate, which was also verified by HRTEM (Figure 3(c)) analysis and the fast Fourier transformation pattern (FFT, Figure 3(c) inset). It indicates that the surface of nanosheet is mainly composed of {001} facet, being in good agreement with the XRD analysis. Figures 3(d) and 3(e) show the SEM and TEM images of flowerlike SnS_2, respectively. We can see that each individual flower consists of a large number of nanosheets. Each individual leaf was well crystallized into the single crystalline, the characteristic of which was confirmed by HRTEM (Figure 3(f)) image and the FFT pattern (Figure 3(f) inset). The diffraction spots of the FFT pattern can be indexed as {002} and {100} planes, confirming that the main exposed facets of flowerlike SnS_2 are {010}.

It is known that, for a given crystal, each facet owns a unique surface atomic arrangement and thus a unique electronic configuration [25]. Therefore, a single crystal exposed with different crystal facets will exhibit different electronic structures. To study the electronic band structures of SnS_2 samples, we measured both the UV-vis absorption spectra and the valence band XPS spectra. From the UV-vis diffuse reflectance spectra as shown in Figure 4(a) we obtained that the main absorption edges of sheetlike SnS_2 and flowerlike SnS_2 are nearly 550 nm and 600 nm, respectively. Correspondingly, the band gaps are calculated to be ~2.25 eV for sheetlike SnS_2 and ~2.05 eV for flowerlike SnS_2, as shown by the plots of transformed Kubelka-Munk function versus the energy of photon (Figure 4(a), inset), being consistent with that of a previous study [26]. The valence band XPS spectra (Figure 4(b)) show that the VB edge of sheetlike SnS_2 is almost the same as that of flowerlike SnS_2, implying that the different band gap energies of sheetlike and flowerlike SnS_2 are due to the different conduction band edges of these two SnS_2 samples: the CB edge of sheetlike SnS_2 is higher than that of flowerlike SnS_2.

Based on the above experimental results, we can draw a scheme of the band structures of sheetlike SnS_2 and flowerlike SnS_2 as shown in Figure 5. Due to their different band structures, especially the conduction band edges, the sheetlike SnS_2 and flowerlike SnS_2 are expected to exhibit different photocatalytic properties.

Photocatalytic activity of the SnS_2 samples was evaluated by performing methyl orange (MO) degradation under visible light irradiation ($\lambda > 420$ nm). The characteristic absorption of MO at $\lambda = 464$ nm was used to monitor the photocatalytic degradation process. It is interesting to note from Figure 6 that although the specific surface area of flowerlike SnS_2 ($32.4\ m^2g^{-1}$) is nearly twice greater than that of the sheetlike SnS_2 ($17.5\ m^2g^{-1}$), its activity for MO degradation is

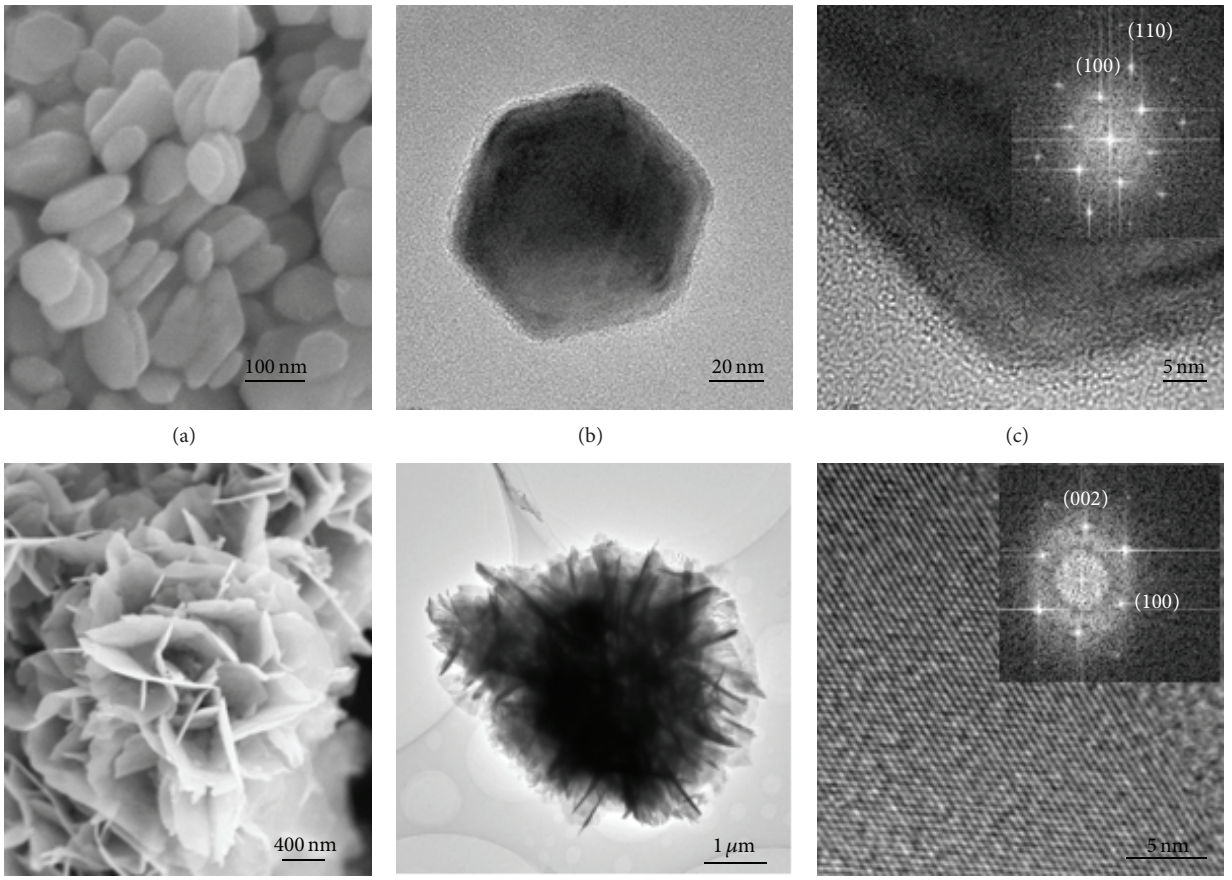

FIGURE 3: SEM, TEM, and HRTEM images of the sheetlike SnS_2 ((a)–(c)) and flowerlike SnS_2 ((d)–(f)). The inset in (c) and (f) is the fast Fourier transform patterns corresponding to the respective HRTEM images.

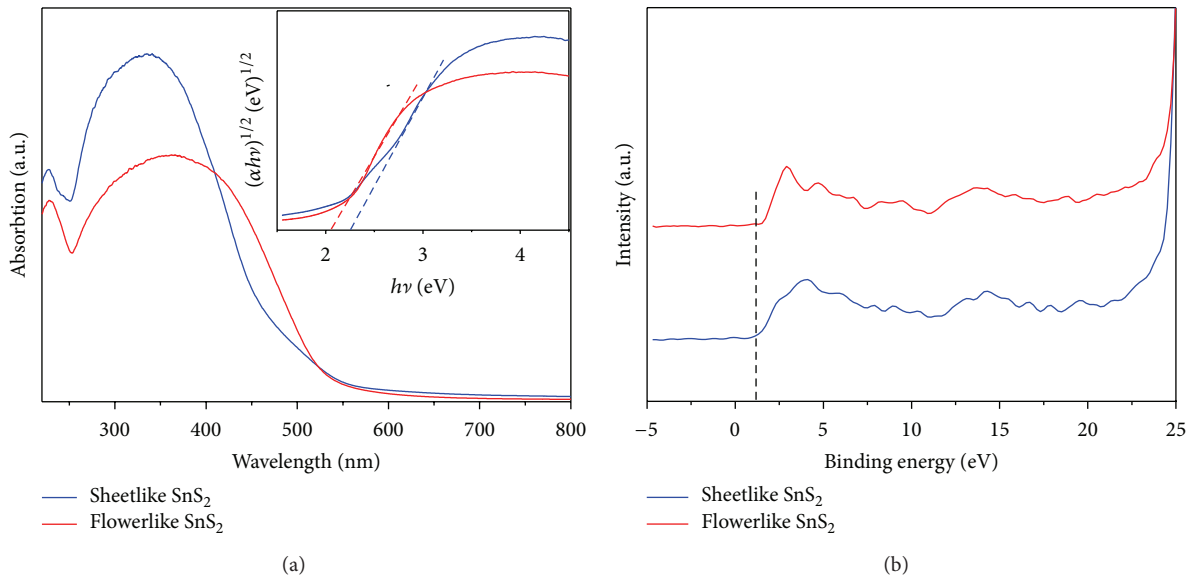

FIGURE 4: (a) UV-visible absorption spectra and corresponding plots of transformed Kubelka-Munk function versus the energy of photon (inset); (b) Valence-band XPS spectra of the two SnS_2 samples.

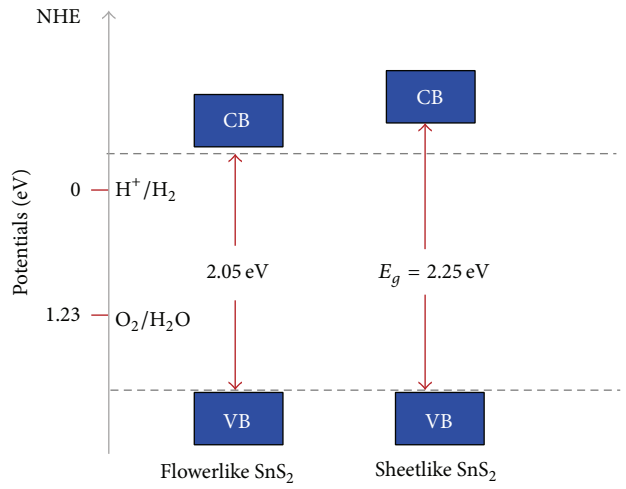

FIGURE 5: Schematic illustration of the electronic band structures of sheetlike and flowerlike SnS_2 samples.

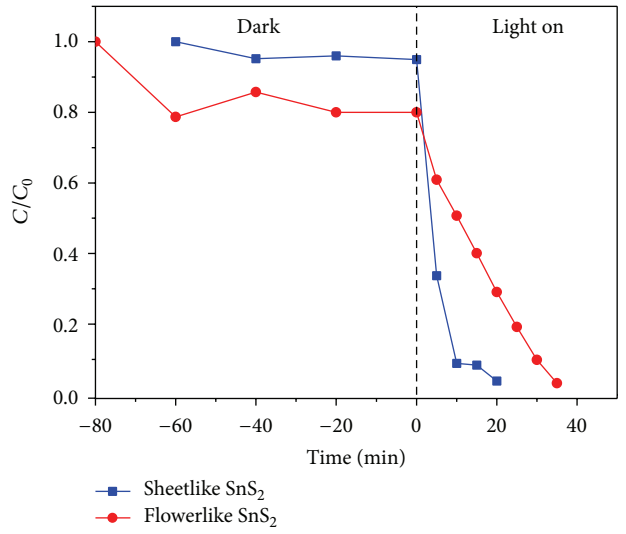

FIGURE 6: Variation of the MO concentration shows the photocatalytic degradation process over two photocatalysts (0.04 g) during dark and upon visible light irradiation ($\lambda > 420$ nm).

substantially lower than that of the sheetlike one. The kinetics of the degradation were fitted to a pseudo first-order reaction: $\ln(C_0/C) = kt$, where k is the apparent rate constant [27]. The apparent rate constant of sheetlike SnS_2 (0.157 min^{-1}) is 2.6 times higher than that of flowerlike SnS_2 (k = 0.06 min^{-1}). It suggests that the photocatalytic activity of SnS_2 is more directly related to its surface structure rather than its specific surface area. Since the SnS_2 of different morphologies possess different predominant facets, the surface atomic structure and thus electronic structure are supposed to play a more deciding role in the different activities.

In order to get further theoretical insight into the mechanism of how the surface atomic structure results in different photocatalytic activities of SnS_2, we calculated the electronic structure and surface stability of sheetlike SnS_2 {001} (S001) and flowerlike SnS_2 {010} (S010) facets through the density functional theory (DFT). In the slab models as illustrated in Figure 7(a), the {010} surface with different determinations is considered. The result shows that, compared to the {010} surface, the {001} surface owns lower surface energy (see Figure S1 in supporting information, available online at http://dx.doi.org/10.1155/2014/394146), meaning that the {001} facet is more stable than the {010} surface. As shown in Figure 7(b), energy band of S001, the conduction band minimum (CBM) of SnS_2 is located at M point of the Brillouin zone and the valence band maximum (VBM) is situated in the region between the K point and the Γ point. This means that SnS_2 is an indirect-gap semiconductor material. In Figures 7(b)–7(d), conduction band edges of S001 and S010 ($S010_s$ and $S010_{Sn}$) are about 1.2 eV, 1.15 eV, and 1.17 eV, respectively, suggesting that the CBM of S001 is more negative than that of S010, being consistent with the previous experimental result (Figure 4(b)). The more negative CBM suggests the stronger reduction ability of photogenerated electrons, resulting in the higher photocatalytic activity of the sheetlike SnS_2. Previous study on different structures of TiO_2 has shown a similar result that a higher conduction band edge can generate more reductive electrons to generate the superoxide radicals $^{\bullet}O_2^-$ to take part in the photocatalytic reaction [5]. Moreover, Figure 7(b) shows that the conduction band of S001 is very abrupt, indicating enhanced mobility of the electrons and hence a possible advantage for restraining recombination of the charge carriers [28, 29]. In contrast, the conduction band of S010 as shown in Figures 7(c) and 7(d) is very flat, which means electrons are easily localized and their mobility is low. It is well known that the increased charge carrier mobility is favorable for a better photocatalytic activity. Therefore, the superior photocatalytic activity of sheetlike SnS_2 could be ascribed to the favorable energy band structure over that of flowerlike SnS_2 in terms of both the thermal dynamics and kinetics of photocatalytic reaction.

4. Conclusions

Sheetlike SnS_2 single crystal exposed with well-defined {001} facets and flowerlike SnS_2 mainly exposed with {010} facets were prepared through a surfactant-free solvothermal process. Theoretical calculation showed that the surface energy of {010} facets was higher than that of {001} facets. However, the photocatalytic activity of flowerlike SnS_2 was much lower than that of sheetlike SnS_2. XPS measurement and first-principle calculation revealed that the different surface atomic structures resulted in different electronic structures; that is, while the valence band maximum of two kinds of samples remained the same, the conduction band minimum of sheetlike SnS_2 was more negative than that of flowerlike SnS_2. The higher conduction band minimum leads to a stronger oxidative ability, and thus a better photocatalytic activity for degradation of MO. Moreover, the higher mobility of the electrons in the more abrupt conduction band of sheetlike SnS_2 also leads to a remarkable enhancement of photocatalytic activity. The present work has provided a deep insight into the role of the surface energy and band structure, both of which are derived from the surface atomic structure, in the photocatalytic activity.

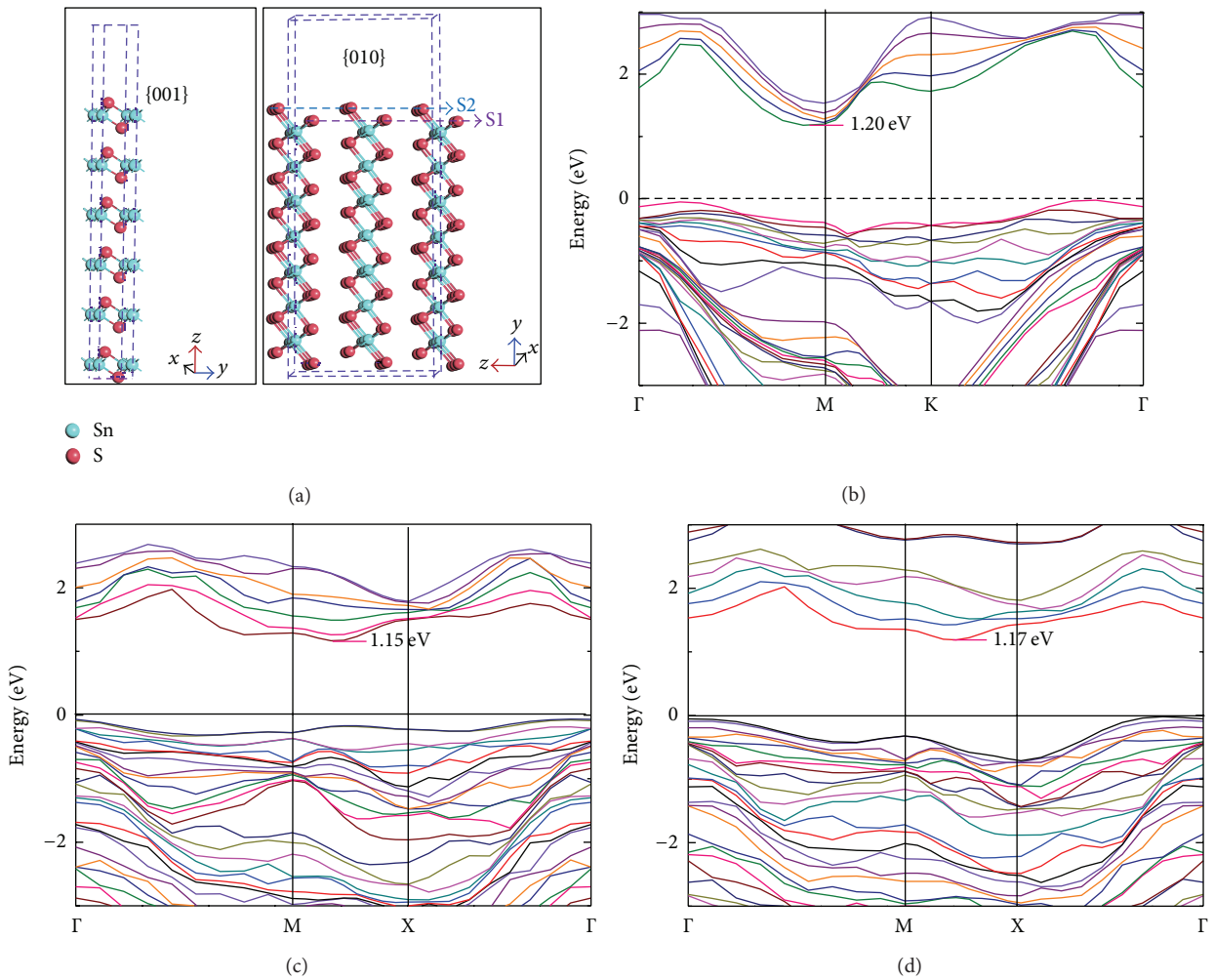

FIGURE 7: (a) Slab models of SnS_2 {001} and {010} surfaces; ((b)–(d)) electronic structures of S001, $S010_s$ and $S010_{sn}$, respectively.

Conflict of Interests

The authors declare that there is no conflict of interests regarding the publication of this paper.

Acknowledgments

This work was supported by the National Basic Research Program of China (973 Program, Contract no. 2014CB239301). Mengyi Li is grateful to Professor Jinhua Ye (NIMS) for hosting her internship visit to NIMS. Gratitude is also to Professor Hua Tong for valuable discussions. Mr. Wei Han (Tianjin Univ.) and Dr. Kun Chang (NIMS) are appreciated for their assistance in materials synthesis and photocatalytic activity evaluation. Calculations were carried out at the Shanghai Supercomputer Center.

References

[1] A. Fujishima and K. Honda, "Photolysis-decomposition of water at the surface of an irradiated semiconductor," *Nature*, vol. 238, no. 1, pp. 37–38, 1972.

[2] F. Seker, K. Meeker, T. F. Kuech, and A. B. Ellis, "Surface chemistry of prototypical bulk II-VI and II Vsemiconductors and implications for chemical sensing," *Chemical Reviews*, vol. 100, no. 7, pp. 2505–2536, 2000.

[3] S. Liu, J. Yu, and M. Jaroniec, "Anatase TiO_2 with dominant high energy 001 facets: synthesis, properties, and applications," *Chemistry of Materials*, vol. 23, no. 10, Article ID 40854093, pp. 4085–4093, 2011.

[4] S. H. Kang, S.-H. Choi, M.-S. Kang et al., "Nanorod-based dye-sensitized solar cells with improved charge collection efficiency," *Advanced Materials*, vol. 20, no. 1, pp. 54–58, 2008.

[5] H. Xu, P. Reunchan, S. Ouyang et al., "Anatase TiO_2 single crystals exposed with high-reactive 111 facets toward efficient H_2 evolution," *Chemistry of Materials*, vol. 25, no. 3, pp. 405–411, 2013.

[6] H. G. Yang, C. H. Sun, S. Z. Qiao et al., "Anatase TiO_2 single crystals with a large percentage of reactive facets," *Nature*, vol. 453, no. 7195, pp. 638–641, 2008.

[7] G. Xi and J. H. Ye, "Synthesis of bismuth vanadate nanoplates with exposed 001 facets and enhanced visible light photocatalytic properties," *Chemical Communications*, vol. 46, no. 11, pp. 1893–1895, 2010.

[8] J. Pan, G. Liu, G. Q. Lu, and H. M. Cheng, "On the true photoreactivity order of {001}, {010}, and {101} facets of anatase TiO_2 crystals," *Angewandte Chemie*, vol. 50, no. 9, pp. 2133–2137, 2011.

[9] W. D. Shi, L. H. Huo, H. S. Wang, H. J. Zhang, and P. H. Wei, "Hydrothermal growth and gas sensing property of flower-shaped SnS_2 nanostructures," *Nanotechnology*, vol. 17, no. 12, pp. 2918–2924, 2006.

[10] K. Chang, Z. Wang, G. Huang, H. Li, W. Chen, and J. Y. Lee, "Few-layer SnS_2/graphene hybrid with exceptional electrochemical performance as lithium-ion battery anode," *Journal of Power Sources*, vol. 201, pp. 259–266, 2012.

[11] F. R. Tan, S. C. Qu, and X. B. Zeng, "Preparation of SnS_2 colloidal quantum dots and their application in organic/inorganic hybrid solar cells," *Nanoscale Research Letters*, vol. 6, no. 1, pp. 298–291, 2011.

[12] Y. Sun, H. Cheng, S. Gao et al., "Atomically thick bismuth selenide freestanding single layers achieving enhanced thermoelectric energy harvesting," *Journal of the American Chemical Society*, vol. 134, no. 50, pp. 20294–20297, 2012.

[13] H. Zhong, G. Yang, H. Song et al., "Vertically aligned graphene-like SnS 2 ultrathin nanosheet arrays: Excellent energy storage, catalysis, photoconduction, and field-emitting performances," *Journal of Physical Chemistry C*, vol. 116, no. 16, pp. 9319–9326, 2012.

[14] J. F. Cao, Z. Xie, X. B. Duan et al., "Visible-light driven photocatalytic and photoelectrochemical properties of porous $SnS_x (x = 1, 2)$ architectures," *CrystEngComm*, vol. 14, no. 9, pp. 3163–3168, 2012.

[15] H. J. Chang, E. In, K. J. Kong, J. O. Lee, Y. M. Choi, and B. H. Ryu, "First-principles studies of SnS_2 nanotubes a potential semiconductor nanowire," *Journal of Physical Chemistry B*, vol. 109, no. 1, pp. 30–32, 2005.

[16] J. Xia, G. C. Li, Y. C. Mao, Y. Y. Li, P. K. Shen, and L. P. Chen, "Hydrothermal growth of SnS_2 hollow spheres and their electrochemical properties," *CrystEngComm*, vol. 14, no. 13, pp. 4279–4283, 2012.

[17] J. Ma, D. Lei, X. Duan et al., "Designable fabrication of flower-like SnS 2 aggregates with excellent performance in lithium-ion batteries," *RSC Advances*, vol. 2, no. 9, pp. 3615–3617, 2012.

[18] A. Yella, E. Mugnaioli, M. Panthöfer, H. A. Therese, U. Kolb, and W. Tremel, "Bismuth-catalyzed growth of SnS_2 nanotubes and their stability," *Angewandte Chemie—International Edition*, vol. 48, no. 35, pp. 6426–6430, 2009.

[19] J. W. Seo, J. T. Jang, S. W. Park, C. Kim, B. Park, and J. Cheon, "Two-dimensional SnS2 nanoplates with extraordinary high discharge capacity for lithium ion batteries," *Advanced Materials*, vol. 20, no. 22, pp. 4269–4273, 2008.

[20] Y. Ji, H. Zhang, X. Ma, J. Xu, and D. Yang, "Single-crystalline SnS_2 nano-belts fabricated by a novel hydrothermal method," *Journal of Physics Condensed Matter*, vol. 15, no. 44, pp. L661–L665, 2003.

[21] Y.-T. Lin, J.-B. Shi, Y.-C. Chen, C.-J. Chen, and P.-F. Wu, "Synthesis and characterization of tin disulfide (SnS_2) nanowires," *Nanoscale Research Letters*, vol. 4, no. 7, pp. 694–698, 2009.

[22] M. Fuchs and M. Scheffler, "Ab initio pseudopotentials for electronic structure calculations of poly-atomic systems using density-functional theory," *Computer Physics Communications*, vol. 119, no. 1, pp. 67–98, 1999.

[23] M. Bockstedte, A. Kley, J. Neugebauer, and M. Scheffler, "Density-functional theory calculations for poly-atomic systems: electronic structure, static and elastic properties and ab initio molecular dynamics," *Computer Physics Communications*, vol. 107, no. 1–3, pp. 187–222, 1997.

[24] Y. C. Zhang, Z. N. Du, K. W. Li, and M. Zhang, "Size-controlled hydrothermal synthesis of SnS_2 nanoparticles with high performance in visible light-driven photocatalytic degradation of aqueous methyl orange," *Separation and Purification Technology*, vol. 81, no. 1, pp. 101–107, 2011.

[25] J. Pan, X. Wu, L. Wang, G. Liu, G. Q. Lu, and H.-M. Cheng, "Synthesis of anatase TiO_2 rods with dominant reactive 010 facets for the photoreduction of CO_2 to CH_4 and use in dye-sensitized solar cells," *Chemical Communications*, vol. 47, no. 29, pp. 8361–8363, 2011.

[26] M. A. Butler, " Photoelectrolysis and physical properties of the semiconducting electrode WO_2," *Journal of Applied Physics*, vol. 48, no. 5, pp. 1914–1920, 1977.

[27] S. C. Yan, Z. S. Li, and Z. G. Zou, "Photodegradation of rhodamine B and methyl orange over boron-doped g-C_3N_4 under visible light irradiation," *Langmuir*, vol. 26, no. 6, pp. 3894–3901, 2010.

[28] S. X. Ouyang, H. T. Zhang, D. F. Li, T. Yu, J. H. Ye, and Z. G. Zou, "Electronic structure and photocatalytic characterization of a novel photocatalyst $AgAlO_2$," *Journal of Physical Chemistry B*, vol. 110, no. 24, pp. 11677–11682, 2006.

[29] S. X. Ouyang, Z. S. Li, Z. Ouyang, T. Yu, J. H. Ye, and Z. G. Zou, "Correlation of crystal structures, electronic structures, and photocatalytic properties in a series of Ag-based oxides: $AgAlO_2$, $AgCrO_2$, and Ag_2CrO_4," *Journal of Physical Chemistry C*, vol. 112, no. 8, pp. 3134–3141, 2008.